Environ Fluid Mech
DOI 10.1007/s10652-013-9300-9

ORIGINAL ARTICLE

Plume rise and spread in buoyant releases from elevated sources in the lower atmosphere

M. Marro · P. Salizzoni · F. X. Cierco · I. Korsakissok · E. Danzi · L. Soulhac

Received: 5 March 2013 / Accepted: 18 July 2013

Abstract This study focuses on the influence of emission conditions—velocity and temperature—on the dynamics of a buoyant gas release in the atmosphere. The investigations are performed by means of wind tunnel experiments and numerical simulations. The aim is to evaluate the reliability of a Lagrangian code to simulate the dispersion of a plume produced by pollutant emissions influenced by thermal and inertial phenomena. This numerical code implements the coupling between a Lagrangian stochastic model and an integral plume rise model being able to estimate the centroid trajectory. We verified the accuracy of the plume rise model and we investigated the ability of two Lagrangian models to evaluate the plume spread by means of comparisons between experiments and numerical solutions. A quantitative study of the performances of the models through some suitable statistical indices is presented and critically discussed. This analysis shows that an additional spread has to be introduced in the Lagrangian trajectory equation in order to account the dynamical and thermal effects induced by the source conditions.

Keywords Atmospheric turbulence · Buoyancy flows · Lagrangian models · Pollutant dispersion · Plume rise

M. Marro (✉) · P. Salizzoni · F. X. Cierco · L. Soulhac
Laboratoire de Mécanique des Fluides et d'Acoustique, Université de Lyon, CNRS UMR 5509
Ecole Centrale de Lyon, INSA Lyon, Université Claude Bernard, 36, avenue Guy de Collongue,
69134 Ecully, France
e-mail: marro.massimo@ec-lyon.fr

I. Korsakissok
Institut de Radioprotection et de Sûreté Nucléaire (IRSN), PRP-CRI, SESUC,
BMTA, 92262 Fontenay-aux-Roses, France

E. Danzi
Departement of Material Science and Chemical Engineering, Politecnico di Torino,
Corso Duca degli Abruzzi 24, 10129 Turin, Italy

Published online: 04 August 2013

1 Introduction

Gas emissions from incinerators, power station stacks and many other pollutant sources are characterised by higher vertical velocity and temperature than the ambient air. This induces the plume centre of mass to rise and the mixing with the surrounding air to increase. In order to evaluate the impact of the pollutant sources on the air quality at the ground level, these release conditions have a great influence because they increment the dilution of pollutant and, consequently, may induce reduced concentrations at the receptors.

The source conditions have two main effects on the plume dynamics and pollutant dispersion: (1) they influence the trajectory of the plume centre of mass producing the plume rise phenomenon; (2) they provide a local production of turbulence that results in higher mixing with the ambient air (and therefore higher plume spreading) with respect to that due to the atmospheric turbulence only. A correct modelling of both effects is required in order to estimate the concentration distribution of the pollutant emitted from the stack.

In the Gaussian atmospheric dispersion models these effects are generally taken into account. The plume rise is simulated by means of a virtual source [23,34], whose position is computed through analytical models, or by the numerical resolution of a system of ordinary differential equations, that describe the time averaged space evolution of the trajectory of the centre of mass of the plume [6]. The plume spread due to the local production of turbulence is modelled by adding to the turbulent diffusivity a term depending on the local generation of turbulence produced by the dynamical and thermodynamical plume conditions [29]. Similarly to other problems concerning turbulent flows, the system of equations is undetermined and it requires some additional equations to model the turbulent fluctuation intensity as function of some dynamical parameters of the flow field (e.g. the mean velocity gradients). In most cases the system is closed simply by adopting the well known 'entrainment assumption', assuming that the plume mixing with the surrounding air is due to: (1) mechanisms of local turbulence production related to the buoyant plume dynamics and (2) the effect of the atmospheric turbulence (e.g. [29]).

Gaussian models are attractive for their low computational costs due to the simplicity of the mathematical formulation, that limits the applicability of these models to dispersion processes taking place in relatively simple flows. Due to this well-known shortcoming, Lagrangian models are often required in order to achieve accurate concentration predictions over complex flow configurations (valleys, wake of obstacles, plant and urban canopies, etc...).

Even Lagrangian models however require specific parameterisation to take into account for the effect of the source condition in case of buoyant releases. For this reason, plume rise and spreading modules have been also introduced in Lagrangian stochastic models [1,15,40]. Details on these parameterisations are further discussed in Sect. 3.

Nowadays, a large number of studies have tested the accuracy of plume rise integral models by means of a comparison between numerical solutions and averaged trajectory of the plume centre of mass measured in small scale experiments performed in wind tunnels [9,16] or in water-tanks [8,35]. In particular, Contini et al. [10] show a detailed analysis of the performances of several plume rise models through a comparison with experimental data. Conversely, few works have tested the ability of these dispersion models in evaluating accurately the mean concentration field produced by buoyant plumes in a turbulent atmospheric boundary layer. Among these we cite Webster and Thomson [40] who simulated the light gas release in the Kincaid experimental campaign [5], Anfossi et al. [2] who performed the simulation of dense gas dispersion in the Thorney Island experiment [21], and Kovalets and Maderich [20] who numerically simulated the BURRO experiment [19]. All these authors considered open field experiments. To our knowledge, the studies providing comparisons

between dispersion models and small scale experiences in wind tunnel are rare. An example is given by Schatzmann [33] who validated an integral model by evaluating the concentration decay on the plume axis at increasing distance from the source in wind tunnel experiments. Differently from the measures provided in open field campaigns, the wind tunnel experiments permit a higher control on the flow parameters and a more accurate description of the plume spatial evolution. The aim of this work is to fill this gap. To this purpose we have designed an experimental campaign and used its results to evaluate the accuracy of a Lagrangian dispersion model.

In the following we describe the experimental equipment and the adopted measure techniques (Sect. 2), the developed numerical model (Sect. 3) and we present a detailed comparison between the experimental results and the numerical solutions provided by the dispersion model (Sects. 4 and 5).

2 Wind tunnel experiments

The experiments were performed in the wind tunnel of the Laboratoire de Mécanique des Fluides et d'Acoustique (LMFA) at the Ecole Centrale de Lyon (ECL). We reproduced a physical model of a small scale stack emitting a buoyant plume in a transversal air flow (Fig. 1). For convenience the buoyant plume was produced by a steady release of hot air, rather than with a light gas, since the measurements of a mean temperature with standard thermocouples is easier to perform rather than the measurements of the concentration of a light gas, as for exemple helium (e.g. [22]).

2.1 Similitude conditions

The condition of dynamical similarity of atmospheric dispersion phenomena requires that the pollutant dispersion takes place within a turbulent flow field reproducing the dynamical characteristics of an atmospheric boundary layer. To this purpose, the ground level and inflow conditions are suitably manipulated so that the vertical profiles of mean velocity and the standard deviation of the three velocity components follow self-similar curves characterising a turbulent boundary layer on rough surfaces [27]. A necessary condition for this is that the Reynolds number $Re_{ext} = u_\infty \delta / \nu_a$ is sufficiently large ($10^4 \div 10^5$) to satisfy the asymptotic

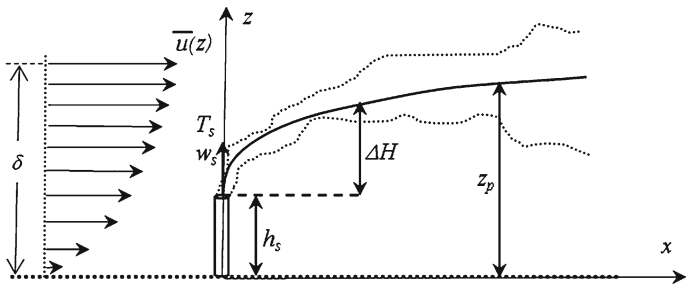

Fig. 1 Interaction between the plume and the external flow characterised by strong mean velocity gradient close to the ground. The continuous line defines the mean trajectory of the plume centre of mass (z_p) as function of the distance from the source; δ is the turbulent boundary layer depth, h_s is the stack height and ΔH is the plume rise due to inertial and thermal effects; w_s and T_s are the velocity and temperature at source, respectively

state $Re_{ext} \rightarrow \infty$; u_∞ is the velocity at the boundary layer height δ and ν_a is the cinematic viscosity of the ambient air. Moreover, the reduced scale simulation of hot gas releases from a stack in an atmospheric neutral boundary layer (Fig. 1) requires further similitude criteria [26,28,31,36]. In general, these are related to the following non-dimensional groups (the subscripts 's' and 'a' are related to the source and ambient air, respectively):

- h_s/δ ratio between the stack height, h_s, and the atmospheric boundary layer depth;
- d_s/δ ratio between the stack diameter, d_s, and the atmospheric boundary layer depth;
- $R = \frac{w_s}{u_\infty}$ ratio between the gas velocity at the stack, w_s, and the free stream velocity at the boundary layer top;
- $Re_{jet} = w_s d_s/\nu_s$, where ν_s is the cinematic viscosity of the emitted gas at the source conditions;
- Froude number $Fr = \frac{u_\infty}{\sqrt{g d_s \frac{\Delta\rho}{\rho_s}}}$ where g is the acceleration of gravity and $\Delta\rho$ is the difference between density of the ambient air, ρ_a, and emitted gas, ρ_s;
- T_s/T_a ratio between the temperature at the source and ambient temperature (equal to ρ_a/ρ_s in low Mach number flows).

Since similarity of Reynolds and Froude number at the source cannot be simultaneously satisfied, the experimental set up has to be designed in order to minimise the influence of Re_{jet}. It is usually assumed that Re_{jet} does not influence the plume dynamics when its value exceeds a critical value Re_{cr} [3,16]. In literature there is not a complete agreement on the value of Re_{cr}. Arya and Lape [3] propose a threshold equal to 2,000 for momentum dominated plumes and around 600 for buoyancy dominated plume; Shahzad et al. [35] report a value of Re_{jet} equal to 4,000 for pure jets and Contini et al. [9] show that Re_{cr} is included within 2,196 and 3,093 for momentum dominated plumes. In our measurements Re_{jet} is in the range 2,060 $\div$ 8,400 and the lowest values of Re_{jet} are related to buoyancy dominated plume. We can therefore conclude that the influence of Re_{jet} on the plume dynamics is negligible.

The d_s/δ parameter has values close to zero and its influence on the mean concentrations is negligible when the distance from the emission point is sufficiently large [13], i.e. $\frac{x}{d_s} > 10$. Conversely, the concentration distribution is very sensitive to h_s/δ, in particular for sources located in the lower part of the atmospheric boundary layer, where the higher velocity gradients take place.

The influence of the ratio T_s/T_a, and therefore of ρ_a/ρ_s, is the object of an important debate in the literature (e.g. [30]) on non-Boussinesq effects in turbulent plumes. Its role in the modifying the flow dynamics is however not fully understood and would require properly designed experiments. This investigation goes beyond the scopes of this study.

Here we restrain our investigation on two parameters: the velocity ratio R and Froude number Fr. To that purpose we consider a fixed geometrical configuration, i.e. fixed d_s/δ and h_s/δ, and we vary the source conditions, T_s and w_s, and the free stream velocity u_∞ to obtain varying R and Fr.

2.2 Experimental equipment and measure techniques

In order to reproduce the characteristic velocity profile of an atmospheric neutral boundary layer in the wind tunnel, we combined the effect of vortex generators and a roughness distribution placed, respectively, at the wind tunnel inlet and on the ground [11,17]. Velocity measurements were performed by means of an X-wire anemometer.

The experimental set up allowed us to simulate a neutral atmospheric boundary layer with a depth $\delta = 0.54$ m and with a free stream velocity u_∞ at its upper boundary that could vary between 0.8 and 1.8 m/s. In these conditions Re_{ext} was included in the range 28,000 ÷ 64,800.

The vertical profile of the longitudinal mean velocity $\overline{u}$ in the lower part of the boundary layer was well fitted by a logarithmic profile of the form:

$$\frac{\overline{u}}{u_*} = \frac{1}{k} \ln\left(\frac{z}{z_0}\right) \tag{1}$$

Where k is the Von Karman constant (equal to 0.4), z_0 is the roughness length and u_* is the friction velocity. In the present study $z_0 = 0.31$ mm. Given this wall roughness the ratio u_*/u_∞ was equal to 0.049. Conversely, a good fit of the mean velocity $\overline{u}$ in the whole extent of the boundary layer was provided by a power law:

$$\frac{\overline{u}}{u_\infty} = \left(\frac{z}{\delta}\right)^n \tag{2}$$

with $n = 0.21$, which represents a typical value for a wind profile in a neutral atmospheric boundary layer [32].

Beside the time averaged profiles of longitudinal velocity (Fig. 2a), the hot-wire measurements provided the standard deviation (Fig. 2b) of the velocity components ($\sigma_u, \sigma_v, \sigma_w$), the Reynolds stress $\overline{u'w'}$, the triple correlations of the velocity components. From the time signals of the instantaneous velocity u we could also estimate the turbulent kinetic energy (t.k.e.) dissipation rate ε (Fig. 2c) as:

$$\varepsilon = 15\nu \frac{1}{\overline{u}^2} \overline{\left(\frac{\partial u'}{\partial t}\right)^2} \tag{3}$$

assuming the turbulence local isotropy and 'frozen turbulence' hypotheses. The reliability of these estimates of ε is proved by the balance of ε and the t.k.e. production term $P = \overline{u_i' u_j'} \frac{d\overline{u}_i}{dx_j}$ shown in Fig. 2c. As we could verify, the divergence of the mean and turbulent fluxes in the t.k.e. budget are negligible compared to P, which therefore has to be balanced by the ε. Since we can reasonably assume that the pressure velocity correlation term in the t.k.e. balance equation is negligible [25], we can therefore conclude that the estimate of ε by means of Eq. (3) is in agreement with that obtained computing the residual of the t.k.e. budget.

The gas was released from a stack model placed in a transversal air flow and it produced an ascending sloping plume (Fig. 1). The source diameter was $d_s = 2.7$ cm and the stack height from the ground was $h_s = 4$ cm. The temperature range of the smokes going out the stack varied between 65 and 150 °C. The gas velocity at the source varied between 2.1 and 6.9 m/s giving Froude number values in the range 2.9–9.6 and velocity ratios R from 1.8 to 6.1. In Table 1 we report the release conditions for the different experimental configurations.

The plume temperature profiles at varying distance from the source were measured by a thermocouple placed on a moving carriage. The measures were performed by evaluating the temperature value averaged over two minutes. We obtain six vertical profiles at increasing distances from the source (Fig. 3) from 0.25 to 2.0 m. In the wind tunnel we also placed two fixed thermocouples at the stack outlet and upwind the source. We used thermocouples of type K and T, characterised by a high thermoelectric coefficient and suitable to measure relatively low temperatures.

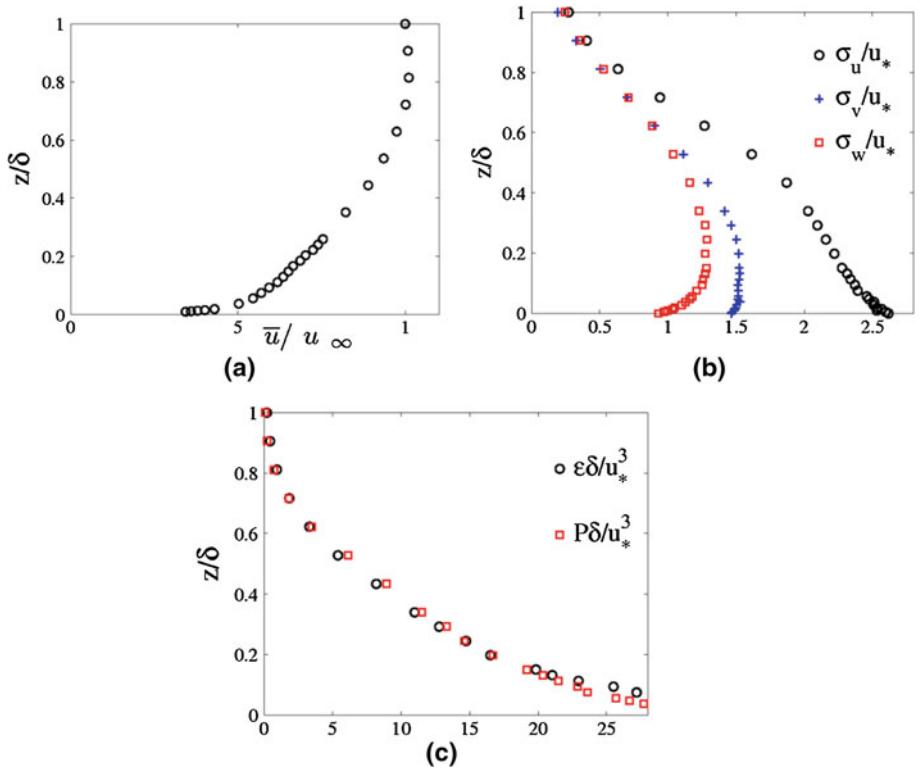

Fig. 2 Non-dimensional profiles of mean velocity (**a**), r.m.s. of the velocity components (**b**) and t.k.e. dissipation rate and t.k.e. production (**c**)

3 Numerical modelling

The plume rise is simulated by an integral model solving the mass, momentum and heat balance equations, similarly to the Gaussian model ADMS [29]. The variables that describe the plume dynamics are obtained by space and time averaging on the transversal sections of the plume.

The effects due to the external air entrainment within the plume are parameterised by the entrainment velocity u_{ent} that linearly depends on the ambient turbulence and on the relative motion between the plume centre of mass and the external velocity. The model assumes a plume with circular cross-section, uniform properties within it and no feedback on the atmospheric turbulence dynamics. The last hypothesis is acceptable if the plume dimensions are significantly lower than the boundary layer depth δ. Other models distinguish the transverse and azimuthal shears in order to consider the influence of the kidney-shaped plume cross-section on the phenomenon [18].

This integral plume model is adopted only in order to compute the centroid trajectory whereas its dilution is computed by means of a Lagrangian stochastic model.

This approach requires simultaneously taking into account the influence of the plume buoyancy on the particles and the independence of the particle motions characterising all the Lagrangian models in anisotropic and inhomogeneous turbulence. For these reasons, following Webster and Thomson [40], we assumed that the mean advection velocity of each

Table 1 Experimental configurations

w_s (m/s)	u_∞ (m/s)	T_s (°C)	T_a (°C)	Fr	R
2.1	0.8	150	26.1	2.9	2.5
2.8		144.5	25.9		3.5
4		144.5	25.6		5.0
4.9		144.1	25.4		6.1
2.2	1.1	134.6	18.2	4	2
5.5		134.6	18.2		5
2.7	1.1	128	25.1	4.2	2.4
3.9		130	24.9		3.6
5.5		128	24.5		5.0
6.6		128	24.2		6.0
2.3	1.1	65	21.6	5.6	2.6
3.4		78	26.3		3.0
4.8		78	26.3		4.3
6.5		78	26.5		5.8
3.6	1.8	98	23.9	8.2	1.9
5.4		98	22.9		2.9
6.9		98	22.3		3.6
3.4	1.8	78	26.2	9.6	1.8
5.1		78	25.8		2.7
6.5		75	24.1		3.4

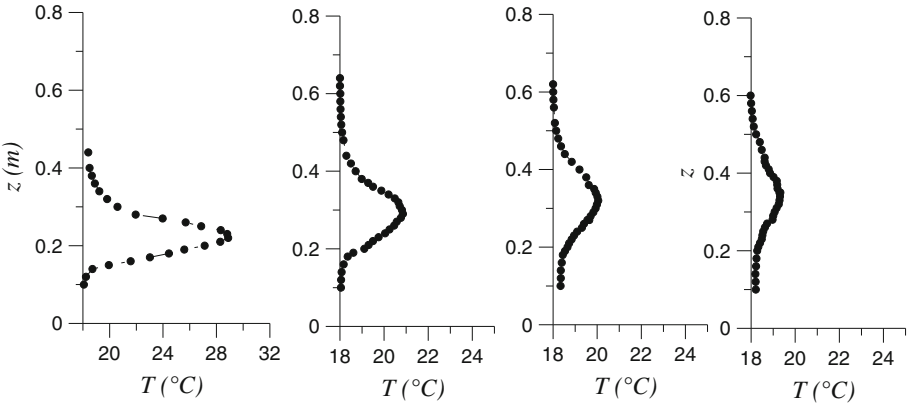

Fig. 3 Experimental profiles of temperature at increasing distance from the source for $Fr = 4$, $R = 2$

particle is equal to the velocity of the plume centre of mass, that was previously computed by an integral plume rise model.

3.1 The integral plume rise model

The model simulates the trajectory of the centre of mass of a plume emitted from a stack with initial temperature and velocity T_s and w_s. The trajectory is computed by integrating the following differential equation:

$$\frac{d\boldsymbol{x}_p}{dt} = \boldsymbol{u}_p \tag{4}$$

where $\boldsymbol{x}_p$ is the location of the plume centre of mass with respect to the source coordinates ($x = 0, y = 0, z = h_s$) and $\boldsymbol{u}_p$ is the velocity of the plume centroid. In the following the subscript 'p' refers to the plume variables and 'a' to those of the ambient flow.

Let us define some quantities that will be used to describe the model more in the detail: the plume mass flux F_m, the momentum flux $\boldsymbol{F}_M$, the heat flux F_h, the buoyancy force $\boldsymbol{B}$ and the aerodynamic drag force $\boldsymbol{D}$:

$$F_m = \pi b^2 \rho_p u_\xi \tag{5}$$

$$\boldsymbol{F}_M = F_m \boldsymbol{u}_p \tag{6}$$

$$F_h = F_m (c_p^p \theta_p - c_p^a \theta_a) \tag{7}$$

$$\boldsymbol{B} = \pi b^2 \boldsymbol{g} (\rho_p - \rho_a) \tag{8}$$

$$D = \frac{1}{2} \rho_a 2\pi b \Delta \boldsymbol{u}_N \left| \Delta \boldsymbol{u}_N \right| C_D \tag{9}$$

where b is the plume radius, $u_\xi = \left| \boldsymbol{u}_p \right|$ is the plume velocity norm, ρ represents the density, c_p the specific heat capacity at constant pressure and θ the potential temperature related to the absolute temperature T through

$$\theta = T \left(\frac{p}{p_0} \right)^{\frac{1-\gamma}{\gamma}} \tag{10}$$

where p is the pressure, p_0 is a reference pressure and $\gamma = \frac{c_p}{c_v}$ is the ratio of the specific heats. C_D is the drag coefficient assumed to be equal to 0.21, $\boldsymbol{g}$ the gravity acceleration vector and $\Delta \boldsymbol{u}_N$ is the relative velocity of the plume perpendicular to the plume axis.

The linear system needed to compute the velocity $\boldsymbol{u}_p$ is given by the following balance equations:

$$\frac{dF_m}{dt} = 2\pi b u_\xi \rho_a u_{ent} \tag{11}$$

$$\frac{dF_{Mx}}{dt} = 2\pi b u_\xi \rho_a u_{ent} u_x^a - u_\xi D_x \tag{12}$$

$$\frac{dF_{My}}{dt} = 2\pi b u_\xi \rho_a u_{ent} u_y^a - u_\xi D_y \tag{13}$$

$$\frac{dF_{Mz}}{dt} = 2\pi b u_\xi \rho_a u_{ent} u_z^a + u_\xi B_z - u_\xi D_z \tag{14}$$

$$\frac{dF_h}{dt} = -\pi b^2 \rho_p u_\xi u_z^p c_p^a \frac{d\theta_a}{dz} \tag{15}$$

If we add the perfect gas equation, we assume as input data the characteristics of the ambient air ($T_a, \theta_a, \rho_a, \boldsymbol{u}_a, c_p^a$) and we neglect the dependence of the specific heat capacity on the temperature and chemical composition ($c_p^p = c_p^a$), we obtain a linear system with 6 equations

and 7 unknowns (T_p, ρ_p, $\boldsymbol{u}_p$, b, u_{ent}). The system closure requires introducing a further equation in order to model the entrainment velocity:

$$u_{ent} = u_{ent}^{rise} + u_{ent}^{turb} \tag{16}$$

The u_{ent}^{rise} component depends on the relative motion between the plume and the external air and it is parameterised as follows:

$$u_{ent}^{rise} = \alpha_1 \left| \Delta \boldsymbol{u}_{\xi} \right| + \alpha_2 \left| \Delta \boldsymbol{u}_N \right| \tag{17}$$

where $\Delta \boldsymbol{u}_{\xi}$ is the relative velocity component along the plume axis. The u_{ent}^{turb} component depends on the turbulent flow field of the ambient air and it is modelled as a function of the flight time t, turbulent kinetic energy dissipation rate ε, vertical velocity fluctuation σ_w and Lagrangian temporal macro-scale T_{Lw}:

$$u_{ent}^{turb} = \alpha_3 \min\left((\varepsilon b)^{1/3}, \sigma_w \left(1 + \frac{t}{2T_{Lw}} \right)^{-1/2} \right) \tag{18}$$

Assuming consistency with the Kolmogorov's turbulence similarity theory, T_{Lw} is usually expressed as [37]:

$$T_{Lw} = \frac{2\sigma_w^2}{C_0 \varepsilon} \tag{19}$$

where C_0 is the Kolmogorov constant assumed to be equal to 4 [41]. The values of the entrainment coefficients are $\alpha_1 = 0.057$, $\alpha_2 = 0.5$ and $\alpha_3 = 0.655$ [29].

The time discretization of the linear system is performed by an explicit Euler scheme. In order to increase the accuracy of the solutions, we implemented an adaptive algorithm. This is based on the information provided by an a posteriori error indicator and it modifies the time step-length in order to control the error due to the time discretisation [4].

It is worth noting that, not all plume rise models in the literature take into account the effect of the dynamic pressure in exerting a drag force on the plume (e.g. [10]). This aspect was discussed in detail by Davidson [12], who showed that neglecting this force in the momentum balance does not necessarily induce to incorrect plume centroid trajectories, provided that appropriate entrainment coefficients are chosen (Eqs. (17) and (18)). However, in this case the integral plume models fails in simultaneously estimating the centroid trajectory and plume spread, over predicting the dilution rate.

The model has been formulated for general atmospheric conditions, characterised by different vertical gradients of potential temperature (Eq. (15)). The model was however tested against an experimental data collected in neutral boundary layer, i.e. with a vertical gradient of the potential temperature equal to zero.

3.2 The Lagrangian stochastic model

The dispersion of pollutant fluid particles around the centre of mass estimated by the plume rise model is computed by the Lagrangian stochastic model SLAM [39]. The temporal evolution of the velocity and position $\boldsymbol{X}$ of each particle is described through the following differential stochastic equations:

$$dU_i' = a_i(\boldsymbol{X}, \boldsymbol{U}', t)dt + b_{ij}(\boldsymbol{X}, \boldsymbol{U}', t)d\zeta_j \tag{20}$$

$$dX_i = (\overline{u}_i + U_i')dt \tag{21}$$

where $\boldsymbol{U}'$ is the Lagrangian velocity fluctuation related to the Eulerian mean velocity $\overline{u}_i$ and $d\zeta_j$ is an incremental Wiener process [14] with zero mean and variance dt. The deterministic acceleration a_i is a function of the statistics of the turbulent flow field and using the well-mixed condition [38] we obtain the following relationship for uncorrelated velocities:

$$a_i = -\frac{U_i'}{T_{Li}} + \frac{1}{2}\frac{\partial \sigma_{ui}^2}{\partial x} + \frac{U_i'}{2\sigma_{ui}^2}\left(U_j \frac{\partial \sigma_{ui}^2}{\partial x_j}\right) \quad i = 1, 2, 3 \tag{22}$$

The stochastic-diffusive term b_{ij} is modelled by means of the Kolmogorov's hypotheses of self-similarity and local isotropy in the spectral inertial sub-range [24]:

$$b_{ij} = \delta_{ij}\sqrt{C_0 \varepsilon} \tag{23}$$

where δ_{ij} is the Kroneker delta. It is worth noting that for sake of simplicity in Eq. (22) the time scale of the autocorrelation of the Lagrangian velocity and the velocity variance are represented as (T_{L1}, T_{L2}, T_{L3}) and $(\sigma_{u1}^2, \sigma_{u2}^2, \sigma_{u3}^2)$, respectively.

The coupling between the Lagrangian model and the integral plume rise model is performed by imposing in Eq. (21) the equality between the Eulerian mean velocity $\overline{\boldsymbol{u}}$ and the velocity of the plume centre of mass $\boldsymbol{u}_p$. More precisely, the plume is considered as made of some puffs that are constituted by a set of particles; at each time step we evaluate the velocity of the puffs by means of the integral model and we associate it to the corresponding particles.

The plume rise, besides influencing the height of the centre of mass, generates some turbulence increasing the plume size. In order to take into account this effect, Webster and Thomson [40] propose to add a random displacement at each time step in Eq. (21). The approach is similar to that of the ADMS model [29] consisting in introducing a second mass conservation equation where the entrainment due to the ambient air turbulence is neglected:

$$\frac{dF_{m0}}{dt} = \frac{d}{dt}(\pi b_0^2 \rho_p u_\xi) = 2\pi b_0 u_\xi \rho_a u_{ent}^{rise} \tag{24}$$

where b_0 depends on time and it represents a measure of the plume radius. We consider an additional spread $\boldsymbol{r} = (r_x, r_y, r_z)$ with zero mean and variance σ^2 depending on the variation of b_0 between two time steps:

$$\sigma^2 = \frac{b_0^2(t + \Delta t) - b_0^2(t)}{4} \tag{25}$$

Now, Eq. (21) assumes the following form:

$$dX_i = (\overline{u}_i + U_i^{'})dt + r_i \tag{26}$$

The formulation of this model is based on two implicit assumptions whose ambiguity deserves to be discussed. First of all, we cannot univocally split the plume width into a part due to the external turbulence and a part due to u_{ent}^{rise}, because the two effects are not linearly additive. Moreover, adding the random displacement $\boldsymbol{r}$, that is a Wiener process, to the trajectories of the particles (Eq. (21)), that is a second-order Markov process, is an empirical procedure which is in contrast with the theoretical bases of the Lagrangian models [14].

4 Validation of the integral model

We tested the plume rise model against the experimental measures of the trajectory of the plume centre of mass $z_p(x)$. In the experiments the location of the centre of mass was estimated by integrating the vertical temperature profiles (Fig. 3):

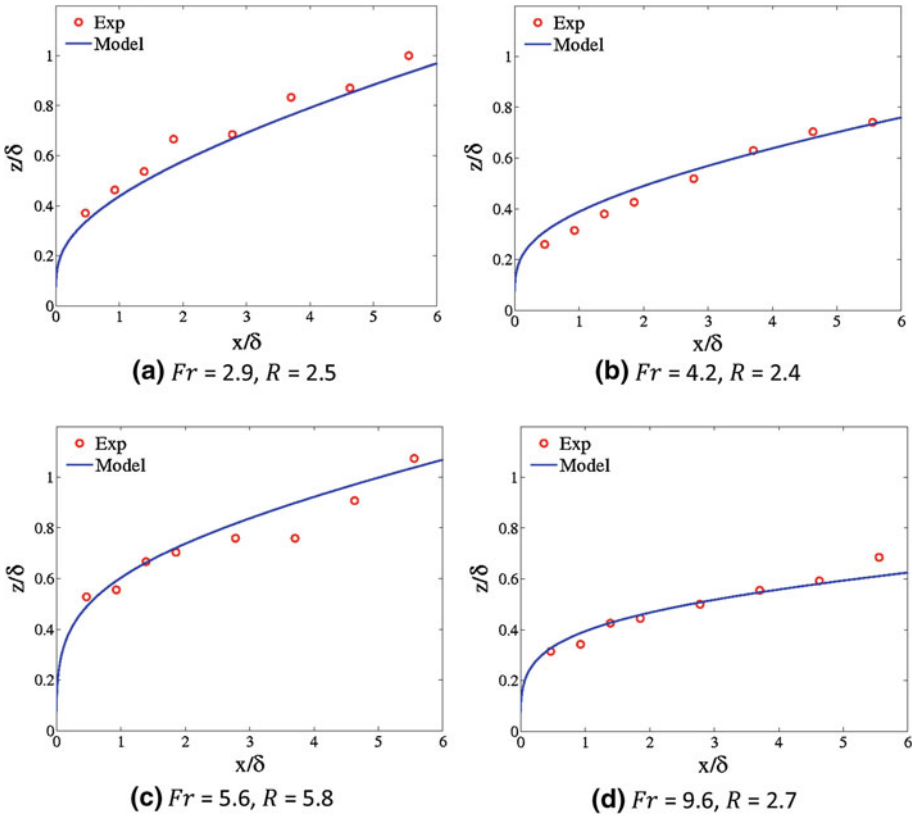

Fig. 4 Trajectory of the plume centre of mass for some configurations: comparison between experimental and numerical values

$$z_p(x) = \frac{\int_0^\infty zT(x,z)dz}{\int_0^\infty T(x,z)dz} \tag{27}$$

The results reported in Fig. 4 show some significant cases at different Froude number and velocity ratio R. We have performed a quantitative evaluation of the accuracy of the numerical results by means of some statistical indices suitable to estimate the consistence between the experimental measures and the solutions provided by the model. These indices, defined in the Appendix, quantify the systematic error, i.e. the global behaviour of the model to overestimate or underestimate the measures, and the local error that provides an estimate of the differences between the single predictions and the mean behaviour of the model. The systematic error is evaluated by the absolute fractional bias (AFB) and geometric mean (MG), whereas the local error is given by the normalised mean square error (NMSE) and geometric variance (VG). A model correctly approximates the experimental data when AFB and NMSE are close to zero and MG and VG are close to 1.

The statistical values reported in Table 2 show that there is a satisfactory agreement between the experimental measures and model results and that the local and systematic errors are low. It is worth noting that the value of AFB reported in Table 2 is similar to those estimated by other authors in testing similar or simpler models. In particular, Contini et al. [10] tested several plume rise models against experiments in water tank and they found

Table 2 Statistical indices for the acceptance of the integral model

AFB	NMSE	MG	VG
0.081	0.011	0.950	1.012

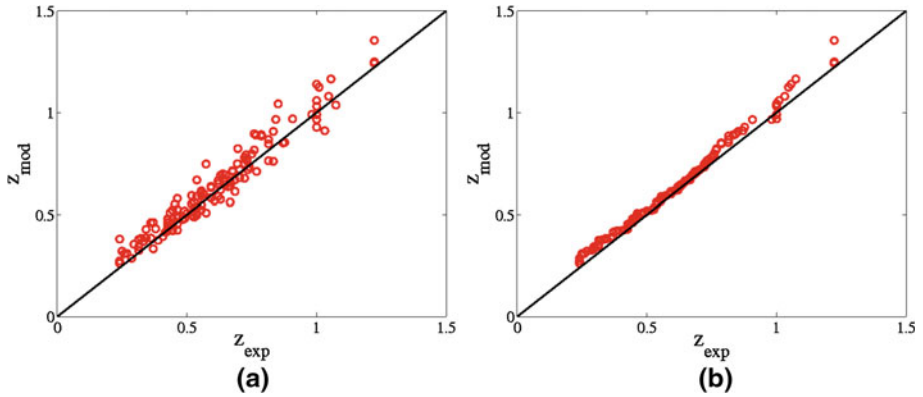

Fig. 5 Scatter plot (**a**) and Q–Q plot (**b**) of the integral model

that the values of AFB were in the range 0.08–0.13 (for neutral conditions). This analysis confirms the reliability of these models in estimating the centroid trajectory.

The statistical analysis of the results is completed by the Scatter Plot that compares directly the experimental data with the modelling values, and the quantile–quantile plot that relates the quantiles of the measures to the quantiles of the numerical solutions comparing the respective probability distributions. In Fig. 5a we report the correlation between the experiments and numerical results for the plume centre of mass (z_{exp}, z_{mod}). The values are localized close to the 1–1 line and, therefore, the agreement between experiments and model is satisfactory. Also the distribution of the quantiles (Fig. 5b) shows the reliability of the model.

5 Validation of the Lagrangian model

In the dispersion modelling we suppose that the molecular diffusion and radiation phenomena are negligible. In such conditions the temperature T (and the mass) of each fluid particle is transported without alteration, i.e. the material derivative $\frac{DT}{dt}$ is equal to zero. Numerical profiles of temperature are compared with the experimentally measured profiles after a suitable adimensionalisation:

$$T^* = \frac{\rho_a c_p^a (T - T_a)}{Q_s} \delta^2 u_\infty \tag{28}$$

where Q_s is the thermal power at the source.

In what follows we compare experimental results with numerical solutions that are computed by means of two different models:

1. a 'classic' Lagrangian model coupled to a plume rise model (Model I).
2. a Lagrangian model that includes both a module simulating the plume rise and a module reproducing the additional spread induced by the production of local turbulence due to thermal and inertial effects (Model II).

The temperature profiles that will be presented in the next subsections are referred to the middle of the plume in the crosswind direction. We restrict our analysis to the vertical dispersion. A similar analysis on the horizontal spread deserves to be further investigated, since its characteristics may differ significantly from those of the vertical spread.

In the statistical analysis, we complete the set of parameters by adding the Fraction of Observations within a factor 2 of prediction (FAC2), as it is customary for atmospheric dispersion models [7]. This is defined as the fraction of data where the ratio between experimental values and numerical solutions is in the range 0.5–2 (see the Appendix).

5.1 Model I

We performed some simulations using the Lagrangian model SLAM in its original formulation, i.e. the particle trajectories are governed by Eq. (21). The results reported in

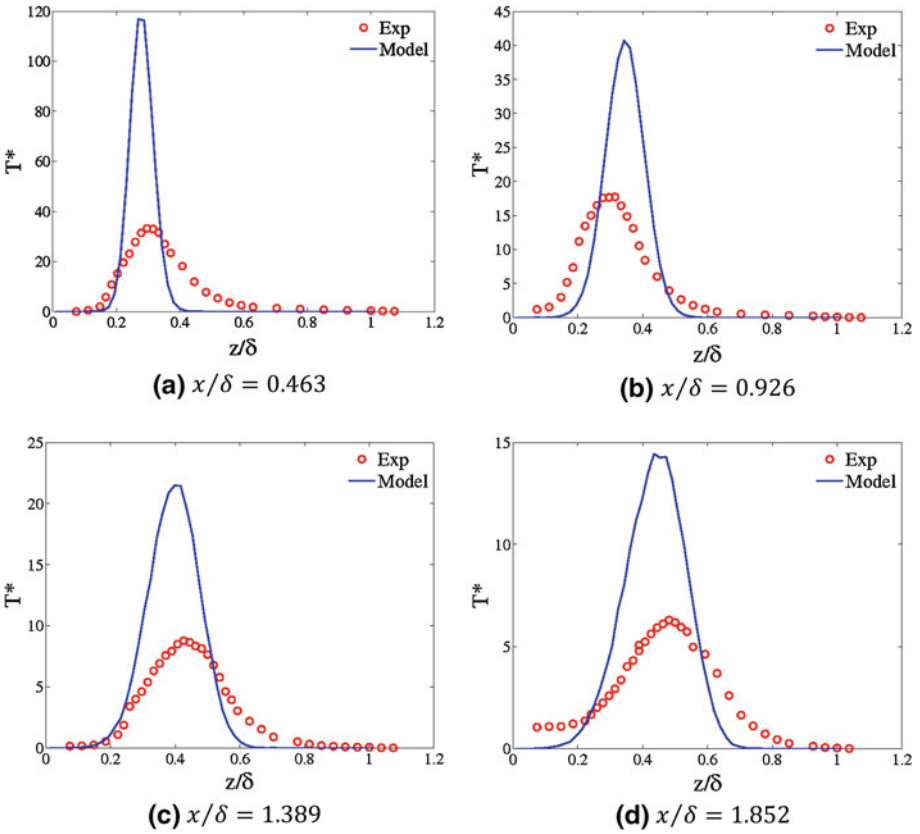

Fig. 6 Comparison of vertical profiles at increasing distance from the source in $Fr = 4$, $R = 2$ configuration; simulations without additional spread

Table 3 Statistical indices of the simulations without additional spread of $Fr = 4$, $R = 2$ configuration

AFB	NMSE	MG	VG	FAC2
0.52	4.62	0.79	2.31	0.401

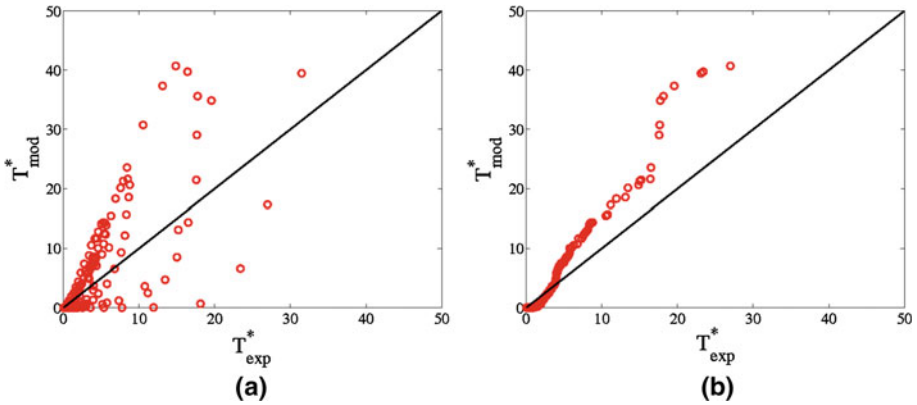

Fig. 7 Scatter plot (**a**) and Q–Q plot (**b**) for $Fr = 4$, $R = 2$ configuration (Model I)

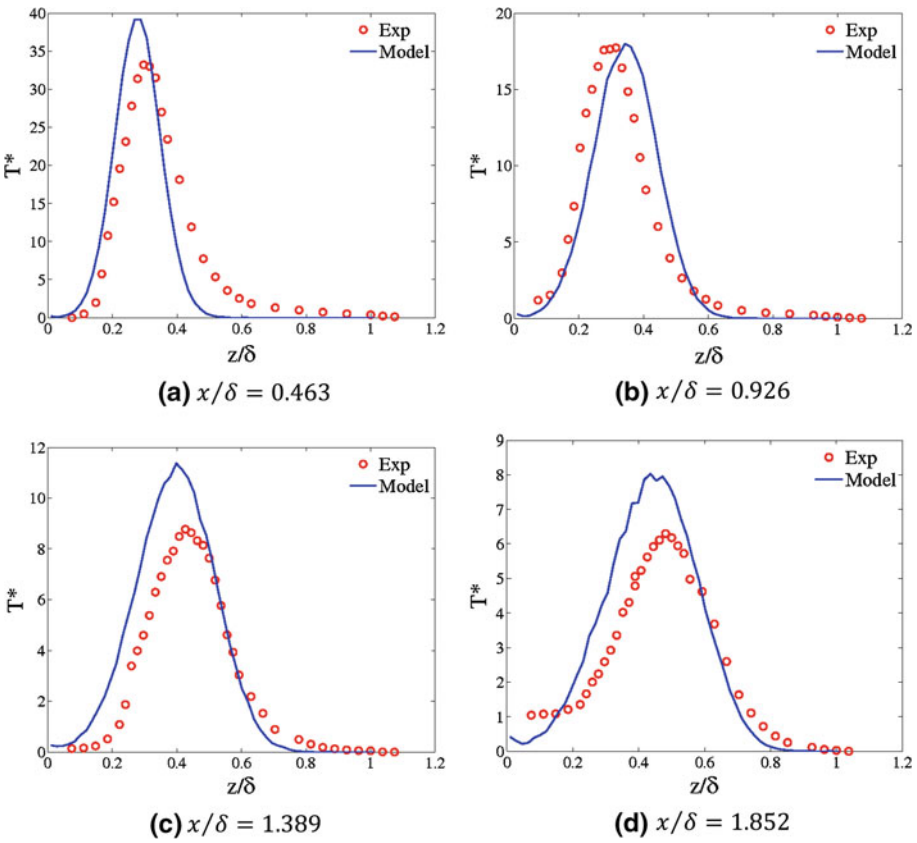

Fig. 8 Comparison of vertical profiles at increasing distance from the source in $Fr = 4$, $R = 2$ configuration; simulations with additional spread

Fig. 6 regard the $Fr = 4, R = 2$ configuration. It is worth noting a significant discrepancy between the measured and numerical profiles varying the distance from the source. The computation of the centre of mass, performed by the integral model inte-

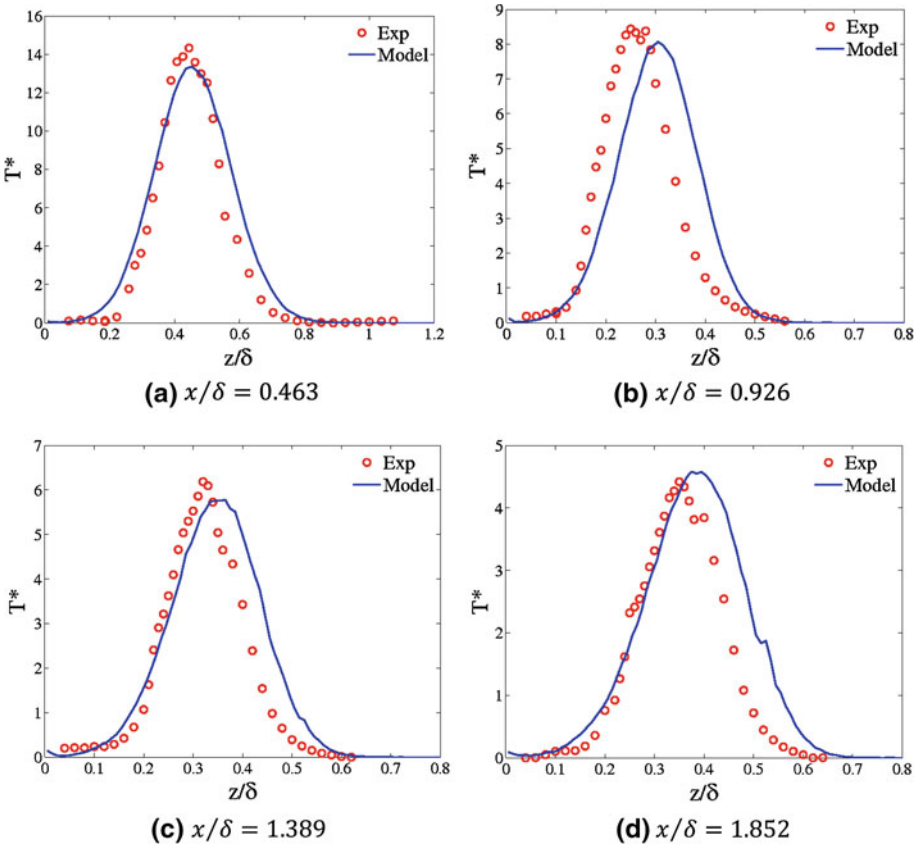

Fig. 9 Comparison of vertical profiles at increasing distance from the source in $Fr = 4$, $R = 5$ configuration; simulations with additional spread

grated in SLAM, clearly provides the same results previously obtained, whereas the modelled dispersion intensity is significantly underestimated along the whole plume length. The statistical indicators reported in Table 3 and the plots in Fig. 7 show a substantial overestimation of the peak temperature by the numerical results and the inability of the model to reproduce the observed temperature profiles. It is clear that the dynamics of the plume are not correctly simulated and some mechanisms influencing the plume dispersion have been neglected.

5.2 Model II

The trajectory of the particles is governed by Eq. (26) where we added a new dispersion term due to the local generation of turbulent fluctuations produced by thermal phenomena; these effects are modelled as a function of the temporal variation of the transversal size of the plume (Sect. 3.2).

Figures 8 and 9 report the non-dimensional profiles at $Fr = 4$, $R = 2$ and $Fr = 4$, $R = 5$ and show that the results computed by the modified model are more accurate and their agreement with the experiments is better.

Table 4 Statistical indices of the simulations with additional spread of $Fr = 4$, $R = 2$ configuration

AFB	NMSE	MG	VG	FAC2
0.133	0.322	0.911	1.503	0.793

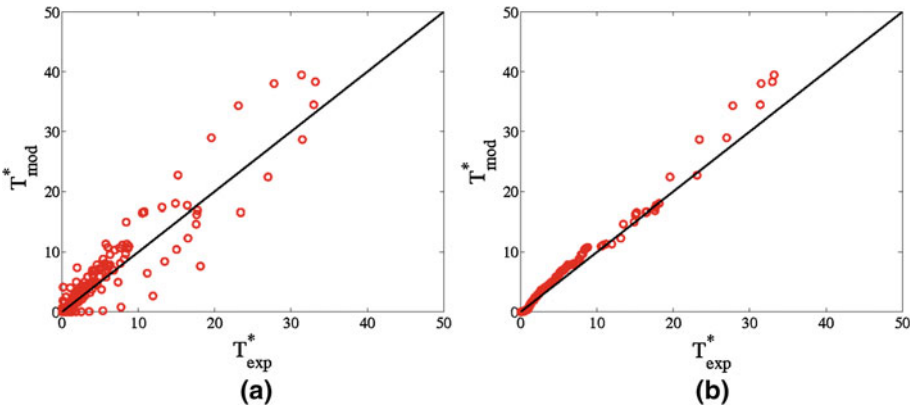

Fig. 10 Scatter plot (**a**) and Q–Q plot (**b**) for $Fr = 4$, $R = 2$ configuration (Model II)

The new simulations show a significant improvement of all the statistical indices (Table 4) with respect to those previously obtained through the old model, where the particle trajectories are governed by Eq. (21).

Figure 10a shows a not negligible dispersion of the data. This distribution is due both to the error coming from the estimate of the plume spread, and to the error provided in the computation of the centre of mass. It is worth noting (e.g. in Fig. 9a) that small errors in the estimate of z_p cause an imperfect overlap of the numerical and experimental profiles of T^* and that can produce a not insignificant local error. The not-optimal value of FAC2 is due to this effect of enlargement of the local error. However, the Q–Q plot (Fig. 10b) shows a distribution of the values close to the 1–1 line with a low dispersion of the data; that means that there is a good statistical agreement between numerical and experimental results.

6 Conclusions

The dispersion of a plume characterised by thermal and inertial phenomena was investigated experimentally and numerically. The aim of the work is to evaluate the accuracy of the results provided by a Lagrangian dispersion model, suitably modified, to simulate the dynamical and thermal effects induced by varying source conditions (velocity and temperature) on the pollutant cloud. The numerical results were compared with the data measured in an experimental small-scale campaign in wind tunnel; we used some statistical indices in order to evaluate the model accuracy from a quantitative point of view.

The trajectory of the plume centre of mass computed by the model presents a very good agreement with that obtained experimentally. On the contrary, there is a significant discrepancy between numerical solutions and experimental data regarding the plume spread when we use the original model (Eq. (21)); the systematic underestimation of the plume spread is due to the fact that the effects of the mechanisms of local turbulence production are neglected.

Such effects are taken into account through an empirical strategy [40]. The new simulations are able to correctly reproduce the increasing of turbulence due to thermal and inertial effects, significantly increasing the accuracy of the numerical results.

Acknowledgements The authors would like to express their gratitude to the laboratory expertise of Christian Nicot.

Appendix

The evaluation of the accuracy of a model requires defining some parameters in order to quantify the differences between numerical solutions and experimental data. In this study we have applied the criteria proposed by Chang and Hanna [7]. The global error is split into a systematic error and a local error. The first is related to the general ability of the model to underestimate or overestimate the measures. The second provides an evaluation of the differences between the single predictions and the mean behaviour of the model. The systematic and local errors are evaluated by the AFB and the NMSE, respectively:

$$AFB = \frac{1}{M}\sum_{i=1}^{M}\left[2.0\frac{\sum_{j=1}^{N}\left|C_{exp}(j) - C_{mod}(j)\right|}{\sum_{j=1}^{N}(C_{exp}(j) + C_{mod}(j))}\right]_i$$

$$NMSE = \frac{1}{M}\sum_{i=1}^{M}\left[\frac{\frac{1}{N}\sum_{j=1}^{N}(C_{exp}(j) - C_{mod}(j))^2}{\frac{1}{N}\sum_{j=1}^{N}C_{exp}(j)\frac{1}{N}\sum_{j=1}^{N}C_{mod}(j)}\right]_i$$

where $C_{exp}(j)$ and $C_{mod}(j)$ are, respectively, the experimental measure and the computed value evaluated at each measure point j and for each plume i; N and M are the number of measurements and the number of plumes, respectively.

If the data are distributed on several orders of magnitude, AFB and NMSE give a larger weight to the higher values. In order to balance this effect we define two logarithmic indices, the MG for the systematic error and the VG for the local error:

$$MG = \frac{1}{M}\sum_{i=1}^{M}\left\{\exp\left[\frac{1}{N}\left(\sum_{j=1}^{N}\ln C_{exp}(j) - \sum_{j=1}^{N}\ln C_{mod}(j)\right)\right]\right\}_i$$

$$VG = \frac{1}{M}\sum_{i=1}^{M}\left\{\exp\left[\frac{1}{N}\sum_{j=1}^{N}(\ln C_{exp}(j) - \ln C_{mod}(j))^2\right]\right\}_i$$

The fraction of observations within a FAC2 is related to the ability of the model to provide results without exceeding an upper bound. The FAC2 is defined as the fraction of data having the property $0.5 \leq C_{exp}/C_{mod} \leq 2$.

The criterion of acceptance of the model performances is provided by the validity ranges of the statistical indices [7]:

- $FAC2 \geq 0.5$;
- $AFB \leq 0.3$;
- $0.7 \leq MG \leq 1.3$;
- $NMSE \leq 1.5$;
- $VG \leq 4.0$.

References

1. Anfossi D, Ferrero E, Brusasca G, Marzorati A, Tinarelli G (1993) A simple way of computing buoyant plume rise in a Lagrangian stochastic dispersion model for airborne dispersion. Atmos Environ 27A:1443–1451
2. Anfossi D, Tinarelli G, Nibart M, Olry C, Commanay J (2010) A new Lagrangian particle model for the simulation of dense gas dispersion. Atmos Environ 44:753–762
3. Arya SPS, Lape JF Jr (1990) A comparative study of the different criteria for the physical modelling of buoyant plume rise in a neutral atmosphere. Atmos Environ 24A:289–295
4. Berrone S, Marro M (2010) Numerical investigations of effectivity indices of space–time error indicators for Navier–Stokes equations. Comput Methods Appl Mech Eng 199:1764–1782
5. Bowne NE, Londergan RJ (1983) Overview, results and conclusions for the EPRI plume model validation and development project: plain site. Report EA-3074, EPRI, Palo Alto
6. Briggs GA (1975) Plume rise predictions. Lectures on air pollution and environmental impact analyses. American Meteorological Society, Boston, pp 72–73
7. Chang JC, Hanna SR (2004) Air quality performance evaluation. Meteorol Atmos Phys 87:167–196
8. Contini D, Robins A (2001) Water tank measurements of buoyant plume rise and structure in neutral crossflows. Atmos Environ 35:6105–6115
9. Contini D, Cesari D, Donateo A, Robins AG (2009) Effects of Reynolds number on stack plume trajectories simulated with small scale models in a wind tunnel. J Wind Eng Ind Aerodyn 97:468–474
10. Contini D, Donateo A, Cesari D, Robins AG (2011) Comparison of plume rise models against water tank experimental data for neutral and stable crossflows. J Wind Eng Ind Aerodyn 99:539–553
11. Counihan J (1969) An improved method of simulating an atmospheric boundary layer in a wind tunnel. Atmos Environ 3(2):197–214
12. Davidson GA (1989) Simultaneous trajectory and dilution predictions from a simple integral plume model. Atmos Environ 23:341–349
13. Fackrell JE, Robins A (1982) Concentration fluctuations and fluxes in plumes from point sources in a turbulent boundary layer. J Fluid Mech 117:1–26
14. Gardiner CW (1983) Handbook of stochastic methods for physics chemistry and the natural sciences. Springer, Berlin
15. Heinz S, Van Dop H (1999) Buoyant plume rise described by a Lagrangian turbulence model. Atmos Environ 33:2031–2043
16. Hewett TA, Fay JA, Hoult DP (1971) Laboratory experiments of smokestack plumes in a stable atmosphere. Atmos Environ 5:767–789
17. Irwin H (1981) The design of spires for wind simulation. J Wind Eng Ind Aerodyn 7:361–366
18. Jirka GH (2004) Integral model for turbulent buoyant jets in unbounded stratified flows. Part I: single round jet. Environ Fluid Mech 4:1–56
19. Koopman RP, Baker J, Cederwall RT, Coldwire HC, Hogan WJ, Kamppinen LJ, Kiefer RD, McClure JD, McRae TG, Morgan DL, Morris LK, Span MW (1982) BURRO series data report LLNL/NWC 1980 LNG spill tests, report UCID-19075. LLNL, Livermore
20. Kovalets IV, Maderich VS (2006) Numerical simulation of interaction of the heavy gas cloud with the atmospheric surface layer. Environ Fluid Mech 6:313–340
21. McQuaid J (1985) Heavy gas dispersion trials at Thorney Island. Elsevier, New York
22. Michaux G, Vauquelin O (2009) Density effect on the mixing and the flow pattern of an impinging air–helium jet. Exp Therm Fluid Sci 33(6):976–982
23. Ooms G, Mahieu AP (1981) A comparison between a plume path model and a virtual point source model for a stack plume. Appl Sci Res 36:339–356
24. Pope SB (1987) Consistency conditions for random-walk models of turbulent dispersion. Phys Fluids 30:2374–2379
25. Pope SB (2000) Turbulent flows. Cambridge University Press, New York
26. Poreh M, Kacherginsky A (1981) Simulation of plume rise using small wind tunnel models. J Wind Eng Ind Aerodyn 7:10–14
27. Raupach MR, Antonia R, Rajoplan S (1981) Rough-wall turbulent boundary layers. Appl Mech Rev 44(1):1–25
28. Robins AG (1980) Wind tunnel modelling of buoyant emissions. In: Atmospheric pollution. Proceedings of the 14th International Colloquium, Paris
29. Robins AG, Apsley DD, Carruthers DJ, McHugh CA, Dyster SJ (2009) Plume rise model specification. Technical report, University of Surrey, National Power and CERC
30. Rooney GG, Linden PF (1996) Similarity considerations for non-Boussinesq plumes in an unstratified environment. J Fluid Mech 318:237–250

31. Rutledge KW (1984) Wind tunnel modelling of buoyant plumes. University of Oxford, Oxford
32. Salizzoni P, Soulhac L, Mejean P, Perkins RJ (2008) Influence of a two-scale surface roughness on a neutral turbulent boundary layer. Bound-Layer Meteorol 127:97–110
33. Schatzmann M (1979) An integral model of plume rise. Atmos Environ 13:721–731
34. Scorer R (1978) Environmental aerodynamics. Wiley, London
35. Shahzad K, Fleck BA, Wilson DJ (2007) Small scale modelling of vertical surface jets in cross-flow: Reynolds number and downwash effects. Trans ASME J Fluid Eng 129:311–318
36. Snyder WH (1981) Guideline for fluid modeling of atmospheric diffusion. U.S. Environmental Protection Agency, Washington, DC
37. Tenneks H (1982) Similarity relations, scaling laws and spectral dynamics. A course held in The Hague, pp 37–68
38. Thomson DJ (1987) Criteria of the selection of stochastic models of particle trajectories in turbulent flows. J Fluid Mech 180:529–556
39. Vendel F, Soulhac L, Mejean P, Donnat L, Duclaux O (2011) Validation of the Safety Lagrangian Atmospheric Model (SLAM) against a wind tunnel experiment over an industrial complex area. In: 14th conference on harmonisation within atmospheric dispersion modelling for regulatory purposes, Kos
40. Webster HN, Thomson DJ (2002) Validation of a Lagrangian model plume rise scheme using the Kincaid data set. Atmos Environ 36:5031–5042
41. Wilson JD, Sawford BL (1996) Review of Lagrangian stochastic models for trajectories in the turbulent atmosphere. Bound-Layer Meteorol 78:191–210